Applied Catalysis B: Environmental 218 (2017) 199–207

Contents lists available at ScienceDirect

Applied Catalysis B: Environmental

journal homepage: www.elsevier.com/locate/apcatb

Water dissociation on multimetallic catalysts

José L.C. Fajín[a,*], M. Natália D.S. Cordeiro[a], José R.B. Gomes[b]

[a] Departamento de Química e Bioquímica, Faculdade de Ciências, Universidade do Porto, P-4169-007 Porto, Portugal
[b] CICECO – Aveiro Institute of Materials, Departamento de Química, Universidade de Aveiro, Campus Universitário de Santiago, P-3810-193 Aveiro, Portugal

ARTICLE INFO

Article history:
Received 7 March 2017
Received in revised form 13 June 2017
Accepted 17 June 2017
Available online 19 June 2017

Keywords:
Water gas shift reaction
CO removal
DFT
Heterogeneous catalysis
Multimetallic catalysts

ABSTRACT

DFT based calculations were employed in the study of the dissociation of the water molecule onto copper and nickel (110) and (111) surface models, incorporating two additional metallic elements, because it was found previously that metal alloying leads to strong synergic effects in the catalysis of this reaction. The dissociation reaction was studied on the Pt/Ru/Ni, Pt/Ru/Cu, Rh/Ru/Cu, Ni/Ru/Cu and Al/Zn/Cu combinations, in a total of 25 trimetallic surfaces. Very low activation energy barriers for the dissociation of water were calculated on several of the surface models, suggesting that multimetallic surfaces can be interesting alternatives for catalyzing the dissociation of the water molecule, which is a crucial elementary step in the water gas shift reaction. Encouragingly, the calculations predict a facile dissociation of the water molecule onto the (AlZn)@Cu(111) catalyst model which is in agreement with recent experimental studies where it was found that a $Cu_{0.5}Zn_{0.5}Al_2O_4$ spinel oxide catalyst holds improved activity for the water gas shift reaction.

1. Introduction

The catalysts used nowadays in industry, which have been developed mostly by trial and error approaches, are still presenting several drawbacks that must be solved urgently, namely, low activity or selectivity and environmental problems caused by the toxicity of the catalyst components or by the formation of reaction byproducts. In some cases, these byproducts are pollutants that contribute to the greenhouse effect. In addition to the environmental problems, the high cost of catalysts, the high energy consumption and the low reaction yields associated with the catalytic process or difficulties in catalyst recycling are economic factors motivating the search of new catalysts or the optimization of the characteristics of catalysts already in use; this should be done through a rational design of nanostructured materials with improved selectivity and activity for industrial processes.

Novel catalysts based on multicomponent active phases were suggested for catalytic reactions with interesting activity and selectivity. For instance, the steam reforming of acetic acid toward the H_2 generation was studied on monometallic, bimetallic and trimetallic catalysts by Hu et al. [1]. It was found that the trimetallic catalyst based on Cu-Zn-Co is more active than bimetallic and monometallic catalysts composed by these metals because of a synergic effect between the three elements. The better performance of the trimetallic catalyst is due to the suppression of side reactions and avoidance of coke formation [1]. The authors proposed different roles for the metals: Cu suppresses CO formation, possibly via WGS reaction; Zn promotes the enhancement of the catalytic activity especially at low temperature; Co is the main active species in the reforming process [1].

In the case of the CO oxidation, where the O_2 dissociation assumes a critical role, a Pt-Ru-Sn ternary catalyst [2] was found to have larger CO tolerances than previous platinum based catalysts. Sn is deposited by chemical vapor deposition and found to be mostly in an oxide form and located in the vicinity of Pt and of Ru regions. It was suggested that Sn aids the formation of oxygenated species from water dissociation, which migrate to the Pt and Ru rich regions where the CO is strongly adsorbed (CO is not adsorbed on Sn) [2]. Despite these experimental evidences, the exact mechanism at the microscopic level is unknown. In these situations, computational studies are tremendously important since it is possible to compare the energetics of reactions under similar conditions which is ideal to check the most favorable adsorption, diffusion and reaction steps allowing to elucidate the reaction mechanism. High-throughput and combinatorial approaches were used to find multicomponent catalysts for the CO oxidation and water gas shift (WGS) reactions. Using such approaches, it was derived and optimized a new Ru-Co-Ce catalyst for the CO oxidation reaction and also a new Pt-Fe-Ce catalyst with synergic effect among the three components for the WGS reaction [3]. Pt-Ru-Co catalysts [4] were

* Corresponding author.
E-mail addresses: luiscagide2001@gmail.com, jfajin@fc.up.pt (J.L.C. Fajín).

http://dx.doi.org/10.1016/j.apcatb.2017.06.050
0926-3373/

also checked for the WGS reaction but it was found that the surface composition and the chemical states of the elements in the catalyst drastically change with the reaction moisture and, therefore, improvements are required.

Computational methods are thought for obtaining knowledge in this area of research because they can be used to interpret data arising from on-going experimental studies or to screen new catalysts for a given reaction; this was assumed to be a priority in research by the USA government [5]. This is because computational methods allow with satisfactory accuracy the study, at the atomic level, of active sites on the catalyst models, reaction mechanisms, coverage effects, among other factors that are important to understand the catalytic activity [6,7]. Reactions on solid surfaces have a quite localized character which often allows the representation of particular catalysts with small molecular models, making the problem tractable from a computational point of view. Furthermore, recent advances in computing power enable the study of catalytic reactions on more complex and realistic catalytic models with increasing accuracy [8–11]. Such advances also enable the calculation of full reaction profiles, upon location of intermediate and transition state structures, which is very crucial to understand the activity of a specific catalyst.

Unfortunately, when applied to a large number of systems, such calculations require significant computation times which prevent their use for catalyst screening purposes. Brønsted-Evans-Polanyi (BEP) relationships between the activation energy barrier for a chemical reaction on a catalytic system and a descriptor were suggested for several reactions [6,12–17] occurring both on single transition metal [6,7,12–18] or multimetallic [8,19] surfaces and look very appropriate for fast elimination of low catalytic activity catalyst candidates. Recently, a general relationship was derived for the O—H bond breakage on transition surfaces based on calculations for the O—H bond break in water, alcohols and organic acids [20,21]. The descriptors used in such BEP relationships are quantities that are calculated much more easily than the activation energies, *i.e.*, they require less computational effort with a concomitant speed increase. Thus, descriptors and BEP relationships are thought to be very convenient for the screening of catalysts. Examples of descriptors are the adsorption energies of the reaction products or even the reaction energy (e.g. difference between the energies of the products and the reactants).

The breakage of the first O—H bond in water is the rate determining step (RDS) of the WGS reaction on copper surfaces [18,22]. Here however, the reader should be aware that an elementary reaction step having the highest activation energy barrier is not always granted to be the RDS since several other factors, such as coverage effects, amount of available active sites on the surface, and propensity to occur the reverse reaction, play also important roles in the overall reaction mechanism [23]. The RDS can be defined from the evaluation of the degree of rate control for all the reaction steps as proposed by Campbell et al. in refs. [24,25]. Therefore, the water dissociation may not be the RDS of the WGS on some of the trimetallic surfaces considered in this work.

Under industrial conditions, the WGS reaction proceeds at high and low temperatures on iron oxide stabilized by chromium oxide and on copper catalysts in the form of metal nanoparticles dispersed onto a support [26], respectively. This reaction is very important in the synthesis and steam reforming of alcohols, and can be also useful for cleaning the hydrogen gaseous stream used in fuel cells [27–30]. But the need of high temperatures and the usage of chromium oxide are triggering the search of more convenient catalysts for the WGS reaction. Recently, a ternary catalyst based on the combination of Al/Zn/Cu demonstrated high activity for the WGS reaction at low temperature [31]. In fact, Boumaza et al. found that the $Cu_{0.5}Zn_{0.5}Al_2O_4$ spinel oxide catalyst, because of its easy reduction, presents a reactivity higher than bimetallic catalysts based on the mixture of copper with other metals.

So, based on these advances, we studied the performance of trimetallic surfaces in the catalysis of the water dissociation reaction. The trimetallic surfaces considered are based on the Pt/Ru/Ni, Pt/Ru/Cu, Rh/Ru/Cu, Ni/Ru/Cu and Al/Zn/Cu ternary combinations because pure Pt, Ru, Ni and Rh were proposed as very reactive metals for the water dissociation [6] and Cu, a cheap metal, is the active metal in the industry catalysts for the WGS at low temperature.

2. Catalyst surfaces models and computational details

2.1. Slab models

Trimetallic catalyst models were generated by the substitution of atoms of a monometallic surface slab (matrix), either from copper or nickel, with atoms of two other metals. In the case of the copper and nickel slabs, (111) and (110) surface terminations were chosen as examples of flat and combed surfaces, respectively. The (111) Miller index is the most stable for the surfaces of these two metals. The (110) surfaces present low coordinated atoms which usually increase the surface reactivity toward water dissociation [6,8,20]; thus, the effect of the low coordinated atoms will be also determined for the trimetallic catalysts. Substitutions of matrix atoms by dopant atoms of the elements Pt, Ru, Rh, Al and Zn were done only in the top layer to yield the Pt/Ru/Ni, Pt/Ru/Cu, Rh/Ru/Cu, Ni/Ru/Cu and Al/Zn/Cu ternary combinations. For comparison purposes, a surface slab corresponding to the (100) Miller index was also considered for the most reactive Al/Zn/Cu ternary combination.

The surfaces of these trimetallic catalysts were based on 3×3 slabs (with respect to the minimal unit cell of Cu(111), Ni(111), Cu(110) or Ni(110) surfaces), with thickness corresponding to four metallic layers. In the case of the (111) flat termination, two different models were obtained for each combination of trimetals, *i.e.*, a slab where the dopant atoms are in direct contact (Fig. 1a) or surrounded by atoms of the matrix (Fig. 1b), while in the case of the combed (110) termination, three different catalyst models were considered, *i.e.* models with the two dopant atoms separated in different combs (Fig. 1c) or with the two dopant atoms separated (Fig. 1d) or in direct contact (Fig. 1e) in the same comb. Therefore, for each combination of three metals, five different catalyst possibilities were explored in this work. The different possibilities for molecular adsorption on each model are shown in Fig. 1.

2.2. Computational details

Adsorption energies, activation energy barriers and reaction energies for the water dissociation reaction ($H_2O^* \rightarrow OH^* + H^*$) on the trimetallic catalyst models considered in this work were determined from spin-polarized periodic DFT calculations with the VASP [32–34] computer code. The PW91 generalized gradient approach (GGA) exchange correlation potential [35] was used to compute the electron density and the projected augmented-wave (PAW) method [36,37] was considered to take into account the effect of core electrons in the valence electron density. Valence electronic states were described using a set of plane waves with a cutoff set to 415 eV. A $7 \times 7 \times 1$ Monkhorst-Pack grid of special k-points [38] was considered for the numerical integration in the reciprocal space. The convergence of the results with respect to plane wave cutoff and Monkhorst-Pack grid was checked for some selected adsorption positions on the different catalyst models. PW91 density functional was chosen to permit a direct comparison with results obtained for the water dissociation on monometallic and bimetallic catalysts [6,9] and also due to its good performance in the study of the RO—H bond cleavage on metallic surfaces [21]. Also, the PW91

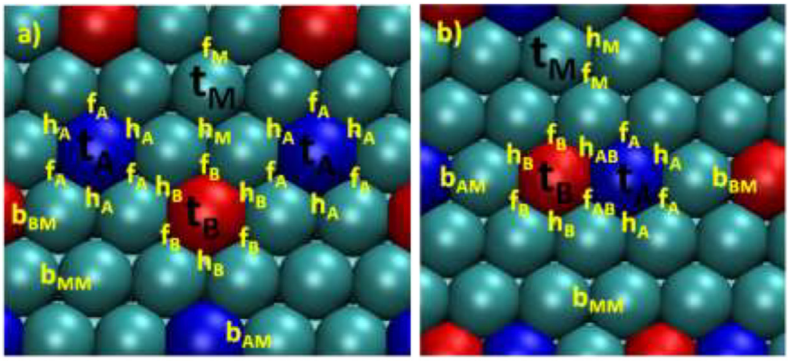

Fig. 1. Adsorption positions at the: a) $(AB)_sM(111)$ surface with dopants atoms A and B separated (M denotes matrix atoms); b) $(AB)_tM(111)$ surface with dopants atoms A and B together; c) $(AB)_{sdc}M(110)$ surface with dopants atoms A and B separated in the different combs; d) $(AB)_{ssc}M(110)$ surface with dopants atoms A and B separated in the same comb and e) $(AB)_{tsc}M(110)$ surface with dopants A and B atoms together in the same comb. Notation for $(AlZn)_t$@Cu(100) single case is analogous to that used for the (111) surfaces.

functional was found to provide results that are similar to those calculated with the PBE approach for adsorption and activation energies of water on Cu(111) [39]. The PBE exchange-correlation functional [40] was used to calculate the energy and geometry for water adsorption in the case of the most interesting combination of metals (*i.e.*, AlZnCu) and the results are found to be very close to those obtained with the PW91 functional. Despite the inclusion of dispersion terms will affect directly the calculated data, van der Waals corrections were not considered in this work because it was recently shown that the preferred reaction route and the rate determining step for the WGS reaction on the Cu(321) surface are the same with or without these corrections [41], *i.e.*, the overall qualitative picture of the general reaction mechanism is unchanged, and also because we want to compare the values reported in this work with results from previous studies where dispersion corrections were not introduced in the calculations [6,9].

The molecular models in the VASP computer code are generated by repetition of a unit cell in the three spatial directions. Therefore, it was introduced a vacuum region in one of the directions to generate the metal slabs. A vacuum region of ~10 Å in the *z* direction was found to be sufficient to avoid spurious interactions of adsorbates with the bottom layer of the metallic slab in the subsequent replica.

Adsorption geometries were obtained by energy minimization with respect to the geometry using a conjugate gradient algorithm for the relaxation of all the atomic positions of the adsorbates and of the two top metal layers. The two bottom metallic layers were kept fixed to simulate the metal bulk.

The transition state (TS) structures for the water dissociation reaction ($H_2O^* \rightarrow OH^* + H^*$) on trimetallic catalyst models were determined with the Dimer approach [42]. Very strict convergence criteria (10^{-6} eV for the total energy change and 10^{-3} eV/Å for the forces) were used. The computation of a single imaginary frequency for the configurations obtained with the Dimer method and visual inspection of the vibration models ensured that those structures were true TS on the potential energy surfaces.

The numerical values for the adsorption energies (E_{ads}) of H_2O and OH + H were obtained by subtraction of the energies of the slab and of gas phase water to the energy of the adsorbate-slab system as follows:

$$E_{ads} = E_{slab-adsorbate} - E_{slab} - E_{H_2O} \quad (1)$$

where $E_{slab-adsorbate}$ is the total electronic energy of the slab-water or slab-(OH + H) systems; E_{slab} is the total electronic energy of the slab and E_{H_2O} is the total electronic gas phase energy of water. Therefore, a negative value of the adsorption energy means favorable adsorption.

Reaction energies (E_{react}) were obtained from the difference between the energies of the products (final states, FS) and of the reactants (initial states, IS) while the activation energy barriers

(E_{act}) were obtained from the difference between the energies of the TS and the IS as follows:

$$E_{react} = E_{slab-OH+H} - E_{slab-H_2O} \quad (2)$$

$$E_{act} = E_{TS} - E_{slab-H_2O} \quad (3)$$

where $E_{slab-OH+H}$, E_{slab-H_2O} and E_{TS} correspond to the total electronic energies of final, initial and transition states, respectively.

All these quantities incorporate the zero point vibrational energy (zpve) corrections that were determined as

$$E_{system+zpve} = E_{system} + \frac{1}{2}\sum_i h * \nu_i \quad (4)$$

based on the harmonic oscillator approach, where $E_{system+zpve}$ corresponds to the corrected zero point vibrational energy of each adsorbate or adsorbate-slab system; E_{system} corresponds to total electronic energy of that adsorbate or adsorbate-slab system (*i.e.* without vibration corrections); h is the Planck constant and υ_i are the values of the vibrational modes of the adsorbate (adsorbed or desorbed, *i.e.* the slab vibrations are not considered).

Estimation of the rate constants for the water dissociation at T = 200 K, 300 K, 400 K, 463 K (typical value for the WGS at low temperature [43]), 500 K, 600 K and 700 K were obtained from the vibrational frequencies of the IS (water adsorbed on the surface) and transition state (TS) structures considering the transition state theory [44] as:

$$k = \left(\frac{k_B T}{h}\right)\left(\frac{q^{\neq}}{q}\right) e^{\frac{-E_{act}}{k_B T}} \quad (5)$$

where k_B is the Boltzmann constant, T is the absolute temperature, h is the Planck constant and E_{act} the activation energy. The terms $q^{\neq}$ and q correspond to the vibrational partition functions for the TS and IS, respectively, which have been approximated from the harmonic vibrational frequencies.

3. Results

In the forthcoming subsections it is described how water and the products of its dissociation (*i.e.*, OH + H) adsorb on the trimetallic surfaces considered and the reactivity of such surfaces toward the water dissociation. The calculated activation energy barriers are then compared with the barriers predicted with a BEP relationship developed in a previous work.

3.1. Adsorption of reactants and products

Adsorption energies (E_{ads}), most stable adsorption sites and shorter distances between adsorbates and surfaces for the adsorption of the water molecule and for the co-adsorption of the OH and H species on the several different adsorption positions on the catalyst models considered in this work are reported in Table 1. Representations of the most stable configurations on each surface for the water molecule can be seen in the leftmost panels of Fig. 2 while for the most stable configurations of the OH + H pair are provided in the rightmost panels of this same figure. The notations for the adsorption sites are provided in Fig. 1.

A complete analysis of the results obtained for water shows that this molecule adsorbs preferentially on top positions through its O atom in all the surfaces. Moderate adsorption energies were calculated with values varying between −0.44 eV on the $(AlZn)_tCu(111)$ surface and −0.76 eV on the $(PtRu)_{sdc}Cu(110)$ surface. From comparison of the water adsorption energies on the five surfaces for each trimetallic combination, it is clear that the presence of low coordinated atoms in the case of the (110) surfaces leads to a strengthening of the water adsorption by ∼0.1 to 0.2 eV with

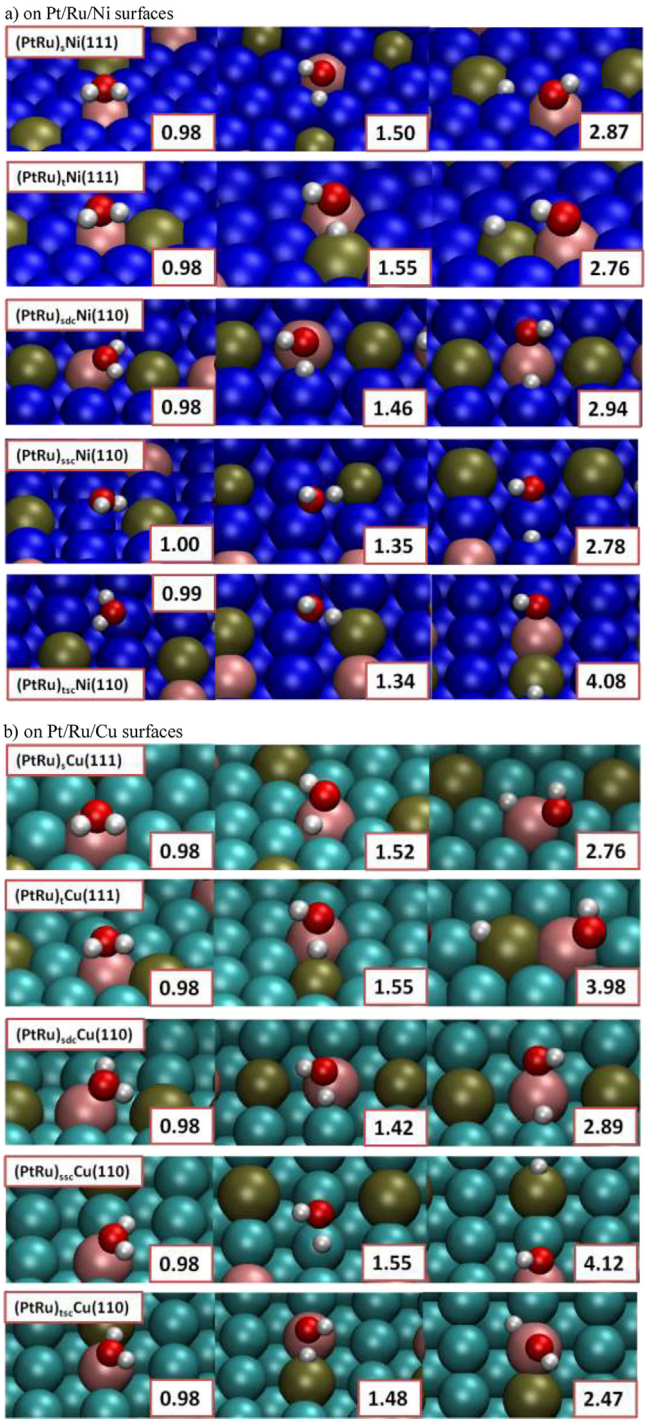

Fig. 2. Optimized structures for the initial (IS), transition (TS) and final (FS) states for the $H_2O^* \rightarrow OH^* + H^*$ reaction on trimetallic surfaces. Length of the cleaved O—H bond is given in Å. Dark blue stands for Ni, clear blue for Cu, pink for Ru, brown for Pt, ochre for Zn, silver for Al and orange for Rh. (For interpretation of the references to colour in this figure legend, the reader is referred to the web version of this article.)
a) on Pt/Ru/Ni surfaces
b) on Pt/Ru/Cu surfaces
c) on Rh/Ru/Cu surfaces
d) on Ni/Ru/Cu surfaces
e) on Al/Zn/Cu surfaces

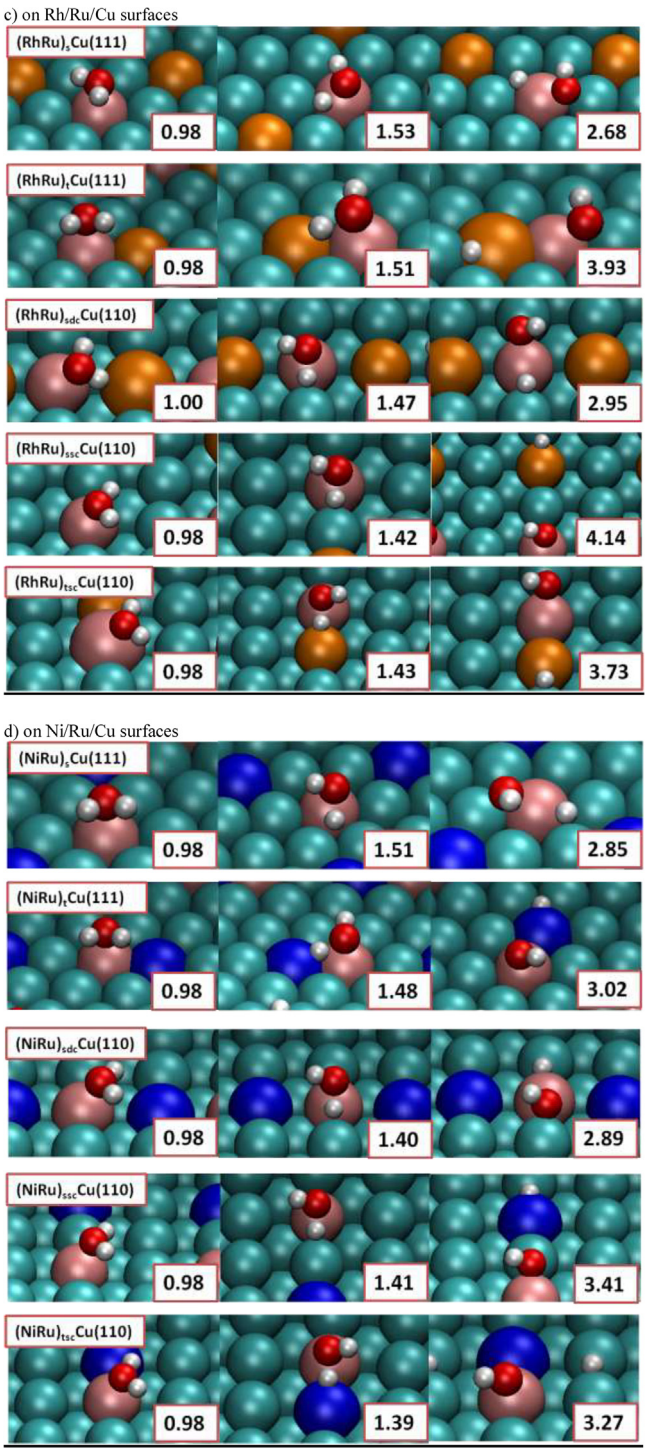

Fig. 2. (*Continued*)

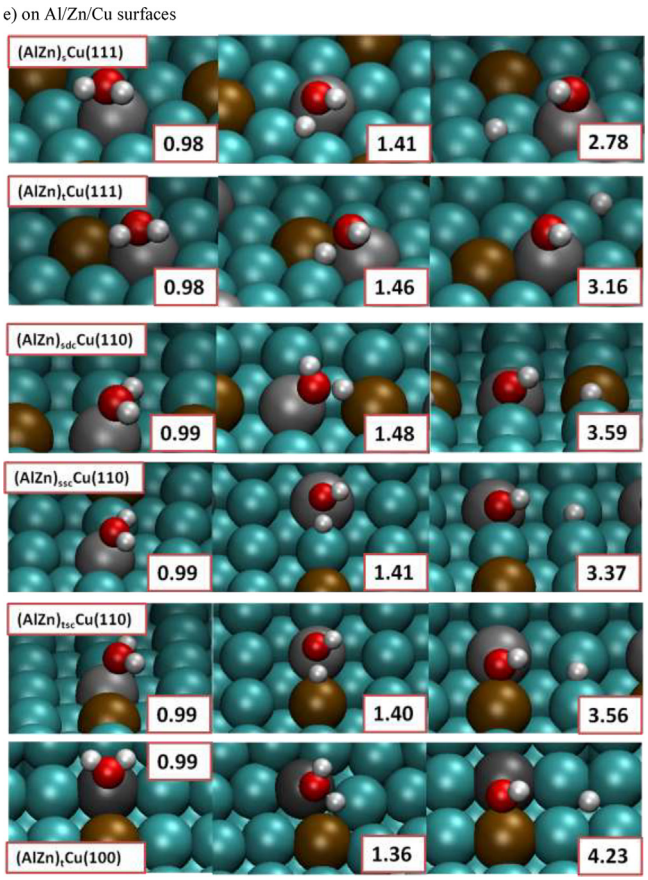

Fig. 2. (*Continued*)

respect to the (111) surfaces and with a concomitant reduction of the adsorbate to surface distances by about 0.1 Å. It has to be also mentioned here that $\mathbf{t_{Al}}$ is the most reactive site for water adsorption on surfaces constituted by the Al/Zn/Cu trimetallic combination while $\mathbf{t}_{Ru}$ is the site that stabilizes more efficiently the water adsorption on most of the surfaces of the other four trimetallic combinations (Pt/Ru/Ni, Pt/Ru/Cu, Rh/Ru/Cu and Ni/Ru/Cu). The exceptions for $\mathbf{t}_{Ru}$ preference are for the water adsorption on $(PtRu)_{ssc}Ni(110)$ and $(PtRu)_{tsc}Ni(110)$ surfaces where adsorption over $\mathbf{t}_{Ni}$ is more favorable. Curiously, the adsorption energy on the later surfaces is approximately ~0.1 eV more negative than on pure Ni(110) surface [6], which is a sign of cooperative effects for the water adsorption on these trimetallic surfaces with respect to the analogous pure nickel surface. Cooperative effects were also found in a previous work [9] for the case of water adsorption on the Rh@Cu(110) bimetallic surface. The results above clearly show that surface doping with Ru atoms leads to increased interactions with the water molecule.

The results concerning the OH + H co-adsorption on the different surfaces are also given in Table 1. The adsorption energies for the OH + H pair are given with respect to the energy of water in gas phase as in previous references [6,9,20,21] to have a common reference for water and OH + H adsorptions. All the adsorption energies present negative values which indicates a thermodynamically favorable reaction with respect to desorbed water and the clean catalyst surfaces. The adsorption energies vary between −0.29 eV on the $(PtRu)_tNi(111)$ surface and −1.52 eV on the $(AlZn)_{tsc}Cu(110)$ surface. It is noticeable that OH preferentially adsorbs on top and bridge positions while H adatoms prefer bridge and hollow sites (see rightmost panels of Fig. 2).

For comparison purposes, the calculations were extended to the $(AlZn)_t$@Cu(100) surface. It is found that the energy and geometry for water adsorption in this surface model are similar to those calculated on the analogous $(AlZn)_t$@Cu(111) surface. The results in Table 1 show that the OH + H pair presents a higher adsorption energy on $(AlZn)_t$@Cu(100) than on the $(AlZn)_t$@Cu(111) surface.

3.2. Activation energy barriers and rate constants for water dissociation

To determine the reactivity of the trimetallic surfaces toward the water dissociation we studied the reaction profile on each sur-

Table 1
Data for the H_2O and OH + H adsorption on the trimetallic surfaces.

Surface[a]	E_{ads}[b] (H_2O)	position[c]	E_{ads}[d] (OH + H)	position (OH/H)[e]
$(PtRu)_sNi(111)$	−0.49	t_{Ru} | (2.33 (Ru))	−0.38	t_{Ru} | (1.92 (Ru))/h_{Pt} | (1.77 (Pt))
$(PtRu)_tNi(111)$	−0.48	t_{Ru} | (2.31 (Ru))	−0.29	t_{Ru} | (1.91 (Ru))/t_{Pt} | (1.59 (Pt))
$(PtRu)_{sdc}Ni(110)$	−0.60	t_{Ru} | (2.30 (Ru))	−1.13	S_{RuNi} | (1.93 (Ni))/S_{RuNi} | (1.67 (Ni))
$(PtRu)_{ssc}Ni(110)$	−0.65	t_{Ni} | (2.07 (Ni))	−0.99	S_{NiNi} | (1.94 (Ni))/S_{NiNi} | (1.58 (Ni))
$(PtRu)_{tsc}Ni(110)$	−0.63	t_{Ni} | (2.08 (Ni))	−1.20	S_{RuNi} | (1.95 (Ni))/S_{PtNi} | (1.70 (Pt))
$(PtRu)_sCu(111)$	−0.54	t_{Ru} | (2.30 (Ru))	−0.53	b_{RuCu} | (2.05 (Cu))/h_{Ru} | (1.68 (Ru))
$(PtRu)_tCu(111)$	−0.52	t_{Ru} | (2.30 (Ru))	−0.66	b_{RuCu} | (2.02 (Ru))/b_{PtCu} | (1.67 (Pt))
$(PtRu)_{sdc}Cu(110)$	−0.76	t_{Ru} | (2.22 (Ru))	−1.35	S_{RuCu} | (1.98 (Cu))/S_{RuCu} | (1.69 (Ru))
$(PtRu)_{ssc}Cu(110)$	−0.66	t_{Ru} | (2.24 (Ru))	−1.22	S_{RuCu} | (2.00 (Ru))/S_{PtCu} | (1.68 (Pt))
$(PtRu)_{tsc}Cu(110)$	−0.62	t_{Ru} | (2.24 (Ru))	−1.44	t_{Ru} | (1.94 (Cu))/h_{Ru} | (1.72 (Ru))
$(RhRu)_sCu(111)$	−0.53	t_{Ru} | (2.31 (Ru))	−0.46	b_{RuCu} | (2.06 (Cu))/h_{Ru} | (1.70 (Ru))
$(RhRu)_tCu(111)$	−0.50	t_{Ru} | (2.30 (Ru))	−0.82	b_{RuCu} | (2.03 (Ru))/b_{RhCu} | (1.72 (Rh))
$(RhRu)_{sdc}Cu(110)$	−0.73	t_{Ru} | (2.21 (Ru))	−1.39	S_{RuCu} | (1.98 (Cu))/S_{RuCu} | (1.69 (Ru))
$(RhRu)_{ssc}Cu(110)$	−0.65	t_{Ru} | (2.24 (Ru))	−1.20	t_{Ru} | (1.91 (Ru))/S_{RhCu} | (1.68 (Rh))
$(RhRu)_{tsc}Cu(110)$	−0.57	t_{Ru} | (2.26 (Ru))	−1.36	S_{RhCu} | (1.70 (Rh))/S_{RuCu} | (2.03 (Ru))
$(NiRu)_sCu(111)$	−0.56	t_{Ru} | (2.30 (Ru))	−0.62	b_{RuCu} | (2.04 (Cu))/h_{Ru} | (1.70 (Ru))
$(NiRu)_tCu(111)$	−0.55	t_{Ru} | (2.29 (Ru))	−0.68	t_{Ru} | (1.93 (Ru))/b_{NiCu} | (1.63 (Ni))
$(NiRu)_{sdc}Cu(110)$	−0.69	t_{Ru} | (2.23 (Ru))	−1.35	S_{RuCu} | (1.99 (Cu))/S_{RuCu} | (1.69 (Ru))
$(NiRu)_{ssc}Cu(110)$	−0.66	t_{Ru} | (2.23 (Ru))	−1.27	S_{RuCu}| (2.01 (Ru))/S_{NiCu}| (1.58 (Ni))
$(NiRu)_{tsc}Cu(110)$	−0.63	t_{Ru} | (2.26 (Ru))	−1.19	t_{Ru} | (1.91 (Ru))/S_{CuCu} | (1.65 (Cu))
$(AlZn)_sCu(111)$	−0.45	t_{Al} | (2.09 (Al))	−0.87	t_{Al} | (1.72 (Al))/f_{Cu} | (1.73 (Cu))
$(AlZn)_tCu(111)$	−0.44	t_{Al} | (2.09 (Al))	−0.88	t_{Al} | (1.73 (Al))/f_{Cu} | (1.73 (Cu))
$(AlZn)_{sdc}Cu(110)$	−0.58	t_{Al} | (2.03 (Al))	−1.40	t_{Al} | (1.80 (Al))/S_{ZnCu} | (1.66 (Cu))
	−0.52[f]	t_{Al} | (2.04 (Al))[f]		
$(AlZn)_{ssc}Cu(110)$	−0.56	t_{Al} | (2.03 (Al))	−1.48	t_{Al} | (1.79 (Al))/S_{CuCu} | (1.66 (Cu))
$(AlZn)_{tsc}Cu(110)$	−0.55	t_{Al} | (2.04 (Al))	−1.52	S_{AlCu} | (1.81 (Al))/S_{CuCu} | (1.66 (Cu))
$(AlZn)_tCu(100)$	−0.45	t_{Al} | (2.09 (Al))	−1.16	b_{AlZn} | (1.82 (Al))/h_{Cu} | (1.79 (Cu))

[a] The last metal indicated is the matrix while the two first metals are the dopants; see Fig. 1 for notation.
[b] *Zero point vibrational* corrected adsorption energy (eV) for water.
[c] Adsorption position for water; in all the cases water is interacting through the O atom with the surface, between parenthesis is given the distance (in Å) between oxygen atom and nearest surface atom.
[d] *Zero point vibrational* corrected adsorption energy (eV) for OH + H.
[e] Adsorption position for OH + H; in all the cases OH is interacting through the O atom with the surface; between parenthesis are given the shorter distances (in Å) between oxygen or hydrogen atoms to nearest surface atom.
[f] Calculated with the PBE exchange-correlation functional.

face model. The TS structures for the most energetically efficient reaction path for the water dissociation on the different trimetallic surface combinations are displayed in the central panels of Fig. 2. The values of the activation energy barriers are given in Table 2 together with estimations of the rate constant for water dissociation at different temperatures and reaction energies. As it can be seen in Table 2, the values of the activation energy barriers are from low to moderate with the lowest and highest values found between 0.19 eV on $(PtRu)_{tsc}Ni(110)$ and 0.62 eV on $(RhRu)_sCu(111)$, respectively. The activation energy barrier values on these surfaces (see Table 2) may be compared directly with those computed on pure Ni(110) and Cu(111) surfaces, with values of 0.39 eV and 0.91 eV [6], respectively, which show an important impact of surface doping on turning more effective the cleavage of the O—H bond in the water molecule.

It is also clear from Table 2 that flat surfaces based on the (111) Miller index present, in general, higher activation energy barriers than combed surfaces with the (110) Miller index because of the presence of atoms with lower coordination in the latter than in the former. The lowest barriers are 0.40 eV, 0.46 eV, 0.45 eV, 0.58 eV and 0.37 eV for (111) surfaces and 0.19 eV, 0.31 eV, 0.39 eV, 0.42 eV and 0.24 eV for (110) surfaces of the PtRuNi, PtRuCu, RhRuCu, NiRuCu and AlZnCu combinations, respectively. So, (110) facets with the PtRuNi combination are the most effective to cleave the O—H bond in the water molecule while in the case of the (111) facets the most active trimetallic catalyst model studied in this work is based on the AlZnCu combination. For the latter trimetallic combination and for comparison purposes, it was also studied the water dissociation on the AlZn@Cu(100) surfaces. We could only perform the calculations for the $(AlZn)_t$@Cu(100) surface, where the Al and Zn dopant atoms are substituting two next-neighbors Cu atoms on the Cu(100) surface because of large surface reconstruction upon the optimization procedure of the surfaces when Zn and Al are not together, *i.e.*, are surrounded by Cu atoms. The results in Tables 1 and 2 confirm that the AlZnCu combination is highly active for the water dissociation reaction.

Since the (111) facets are more stable, their abundance in a realistic catalyst will be larger than those with (110) orientation and, to a lesser extent, than those with (100) orientation. Thus, catalysts based on Al/Zn/Cu should present higher yields of products for water dissociation than those based on the other trimetallic combinations. Encouragingly, a very reactive catalyst based on a mixed oxide of Al/Zn/Cu was recently suggested for the WGS reaction [31] where the water dissociation is a key step.

In the case of the surfaces constituted by Ni/Ru/Cu and Pt/Ru/Ni trimetallic combinations, the activation energy differences are ~0.1–0.2 eV for the dissociation reaction occurring on flat or on combed surfaces.

For surfaces composed by the Pt/Ru/Cu and Rh/Ru/Cu combinations, the $(AB)_sM(111)$ cases present higher activation energy barriers than the $(AB)_tM(111)$ ones and, in some situations, the activation energies on the $(AB)_tM(111)$ surfaces are smaller than on (110) surfaces because of the presence of two dopant atoms in direct contact.

The water dissociation reaction can be limited if the desorption of the reactants (adsorbed water) is easier than the cleavage of the O—H bond, *i.e.*, one may have an idea of how the WGS reaction is prone to occur on a specific catalyst model from the comparison of the activation energy barrier and of the adsorption energy of the reactants. So, adsorption energies higher, in absolute value, than activation energy barriers should prevent desorption of the reactants and favor the surface reaction. The comparison of the E_{act} (Table 2) and E_{ads} (Table 1) for each surface suggests that water desorption is expected to occur only in the less active catalyst

Table 2
Activation energy barrier (E^{o}_{act}, eV), reaction energy (E^{o}_{react}), reaction rate constant (s^{-1}) at 463 K (values at other temperatures are given in Table S1 of SI), imaginary frequency (υ) for transition state (cm^{-1}) and distances (d, Å) for the O—H bond cleaving in [$H_2O^* + * \rightarrow OH^* + H^*$] reaction on several trimetallic surfaces.

Surface[a]	$d_{O\cdots H}$	E^{o}_{act} [b]	$E^{o,BEP}_{act}$ [c]	E^{o}_{react} [b]	k (s^{-1}) [d]	υ
$(PtRu)_sNi(111)$	1.50	0.59	0.63	0.10	2.85×10^{6}	1055.8
$(PtRu)_tNi(111)$	1.55	0.40	0.68	0.20	1.78×10^{8}	621.3
$(PtRu)_{sdc}Ni(110)$	1.46	0.29	0.30	−0.53	2.41×10^{9}	456.8
$(PtRu)_{ssc}Ni(110)$	1.35	0.23	0.36	−0.34	4.05×10^{9}	993.9
$(PtRu)_{tsc}Ni(110)$	1.34	0.19	0.28	−0.57	2.25×10^{10}	980.6
$(PtRu)_sCu(111)$	1.52	0.60	0.57	0.02	1.19×10^{6}	1008.2
$(PtRu)_tCu(111)$	1.55	0.46	0.51	−0.13	1.01×10^{7}	544.9
$(PtRu)_{sdc}Cu(110)$	1.42	0.31	0.21	−0.59	2.47×10^{9}	454.6
$(PtRu)_{ssc}Cu(110)$	1.55	0.47	0.27	−0.56	2.69×10^{7}	1036.4
$(PtRu)_{tsc}Cu(110)$	1.48	0.32	0.21	−0.73	5.49×10^{8}	462.4
$(RhRu)_sCu(111)$	1.53	0.62	0.60	0.07	3.31×10^{6}	1003.1
$(RhRu)_tCu(111)$	1.51	0.45	0.44	−0.33	6.33×10^{7}	657.8
$(RhRu)_{sdc}Cu(110)$	1.47	0.54	0.19	−0.67	1.47×10^{6}	1096.7
$(RhRu)_{ssc}Cu(110)$	1.42	0.46	0.28	−0.54	4.26×10^{7}	1037.3
$(RhRu)_{tsc}Cu(110)$	1.43	0.39	0.20	−0.79	2.15×10^{8}	712.7
$(NiRu)_sCu(111)$	1.51	0.58	0.53	−0.06	2.28×10^{6}	1034.2
$(NiRu)_tCu(111)$	1.48	0.51	0.50	−0.13	1.51×10^{7}	995.5
$(NiRu)_{sdc}Cu(110)$	1.40	0.44	0.21	−0.66	9.88×10^{7}	1072.3
$(NiRu)_{ssc}Cu(110)$	1.41	0.45	0.25	−0.61	8.21×10^{6}	1045.6
$(NiRu)_{tsc}Cu(110)$	1.39	0.42	0.28	−0.56	1.31×10^{8}	1060.7
$(AlZn)_sCu(111)$	1.41	0.37	0.42	−0.41	4.68×10^{8}	1186.3
$(AlZn)_tCu(111)$	1.46	0.44	0.41	−0.44	7.93×10^{7}	933.5
$(AlZn)_{sdc}Cu(110)$	1.48	0.47	0.18	−0.82	3.95×10^{8}	1354.9
$(AlZn)_{ssc}Cu(110)$	1.41	0.37	0.15	−0.92	4.37×10^{8}	874.7
$(AlZn)_{tsc}Cu(110)$	1.40	0.24	0.13	−0.98	1.74×10^{10}	1107.8
$(AlZn)_tCu(100)$	1.36	0.21	0.29	−0.71	7.25×10^{9}	1175.2

[a] The last metal indicated is the matrix while the two first metals are the dopants; see Fig. 1 for notation.
[b] In activation and reaction energies ^{o} stands for ZPV corrected values.
[c] Estimated activation energy barrier values using the general BEP relationship obtained in Ref. 22.
[d] Rate constant values determined using Eq. 1 at 463 K.

models, namely, in the cases of the $(PtRu)_sNi(111)$, $(PtRu)_sCu(111)$, $(RhRu)_sCu(111)$ and $(NiRu)_sCu(111)$ surfaces.

Reaction energies (E_{react}) given in Table 2 indicate that the water dissociation is an endothermic reaction on some of the flat surfaces, viz. on the $(PtRu)_sNi(111)$, $(PtRu)_tNi(111)$, $(PtRu)_sCu(111)$ and $(RhRu)_sCu(111)$ surfaces, while on the others it is an exothermic or thermoneutral reaction. The water dissociation is especially exothermic on Al/Zn/Cu combed surfaces which suggests this to be a very active catalyst for the dissociation of the O—H bond in the water molecule. On the flat surfaces where the reaction is endothermic the reverse reaction is more plausible than the water dissociation.

The data reported in Tables 1 and 2 suggest that Al/Zn/Cu surfaces should be very reactive for the water dissociation. For comparison purposes, the activation energies for the dissociation of the water molecule on the Cu(111) and Cu(110) surfaces are 0.91 eV and 0.61 eV, respectively [6]. A projected density of states (pDOS) analysis along the reaction path on these ternary surfaces was done and compared with the pDOS of clean trimetallic surfaces and the parent undoped Cu surfaces to have an electronic perspective of the catalytic process.

From the pDOS in Fig. 3, it is clear that the doped pristine surfaces present higher amounts of electronic states under the Fermi level than the pure Cu surfaces. A higher electron density is also found for the valence states of (110) terminated surfaces when compared with the (111) Miller index, which can lead to a stronger interaction with adsorbates (if bonding states are filled in the adsorbate). In fact, adsorption of water and OH + H pair is more favorable on combed surfaces than on the flattened ones as can be seen in Table 1.

The pDOS along the reaction path on each surface shows that the water adsorption is characterized by a low hybridization of metal and water levels in agreement with the moderate/low adsorption energies calculated for water adsorption. These observations contrast with those for the co-adsorption of the OH + H pair where the p-band of oxygen and the s-band of hydrogen overlap significantly to the d-band of the metallic system, especially in the case of the (110) Miller index surfaces. An intermediate picture between the IS and FS is found for the TS, and the center of the d-band is pulled to lower energies on going from the initial to the final state.

The reaction energy is clearly correlated with the activation energy barrier, *i.e.*, the water dissociation reaction is more exothermic for the most active surfaces. This observation is in line with results obtained for the same reaction but on single metal and bimetal catalytic surfaces [6,9] where it was possible to determine BEP relationships linking the activation energy barrier with the reaction energy. The reaction energy has been considered as a descriptor in several BEP relationships [45].

Descriptors for the water dissociation were obtained for the reaction on monometallic and bimetallic catalysts in previous works [6,20,21][6,20,21 and references therein]. The (co-)adsorption energy of the reaction products (OH + H) was presented as an adequate descriptor for the reaction of water dissociation both in terms of reaction description and of computational effort needed to its calculation. Therefore, we used the values of OH + H adsorption energy, E_{ads}(OH + H), from Table 1 to estimate the activation energy barrier, E_{act}(HO···H), on the surfaces models considered in this work together with the BEP relationship:

$$E_{act}(HO\cdots H) = 0.4329 \times E_{ads}(OH + H) + 0.7942 \quad (6)$$

taken from Ref. [20]. The estimated values for the E_{act}(HO···H) are given in Table 2.

In the case of the (111) surfaces, the calculated and estimated activation energy barriers are in very good agreement with differences < 0.05 eV. However, in the case of the surface models with (110) termination, the differences between calculated and estimated E_{act}(HO···H) values are quite significant, which suggests that the BEP relationship is not useful for multicomponent stepped surfaces. The calculated rate constants for the water dissociation show that the reaction should be very fast at high temperatures on all the surfaces while at low temperatures fast reaction is only predicted on the (110) surfaces and on a single (111) surface, namely, the $(AlZn)_sCu(111)$ model.

4. Conclusions

The reactivity of trimetallic catalyst model surfaces based on copper and nickel slabs incorporating two additional metals toward the water dissociation was explored through periodic density functional calculations. For comparison purposes, the surfaces considered were cut along the (111) and (110) planes to understand metal coordination effects in flat (coordination number of 9) and combed (coordination number of 7) surfaces, respectively. In general it was found that the combed surfaces display higher reactivity toward the water dissociation than the flat surfaces. Importantly, the catalytic activity of the trimetallic models surfaces studied in this work is high; most of the surfaces considered present low activation energy barriers for water dissociation, the water adsorption energy is higher (in absolute value) than the computed activation energy barrier, which prevents the reactants desorption, and the water dissociation is an exothermic or thermoneutral reaction. Among the different combinations of metal atoms, the calculations suggest that surfaces constituted by Al/Zn/Cu should display important activities towards water dissociation, which is in line with recent experimental findings.

The validity of a BEP relationship derived in a previous work for estimating activation energy barriers of reactions involving the breakage of the O—H bond was analyzed also in this work for the

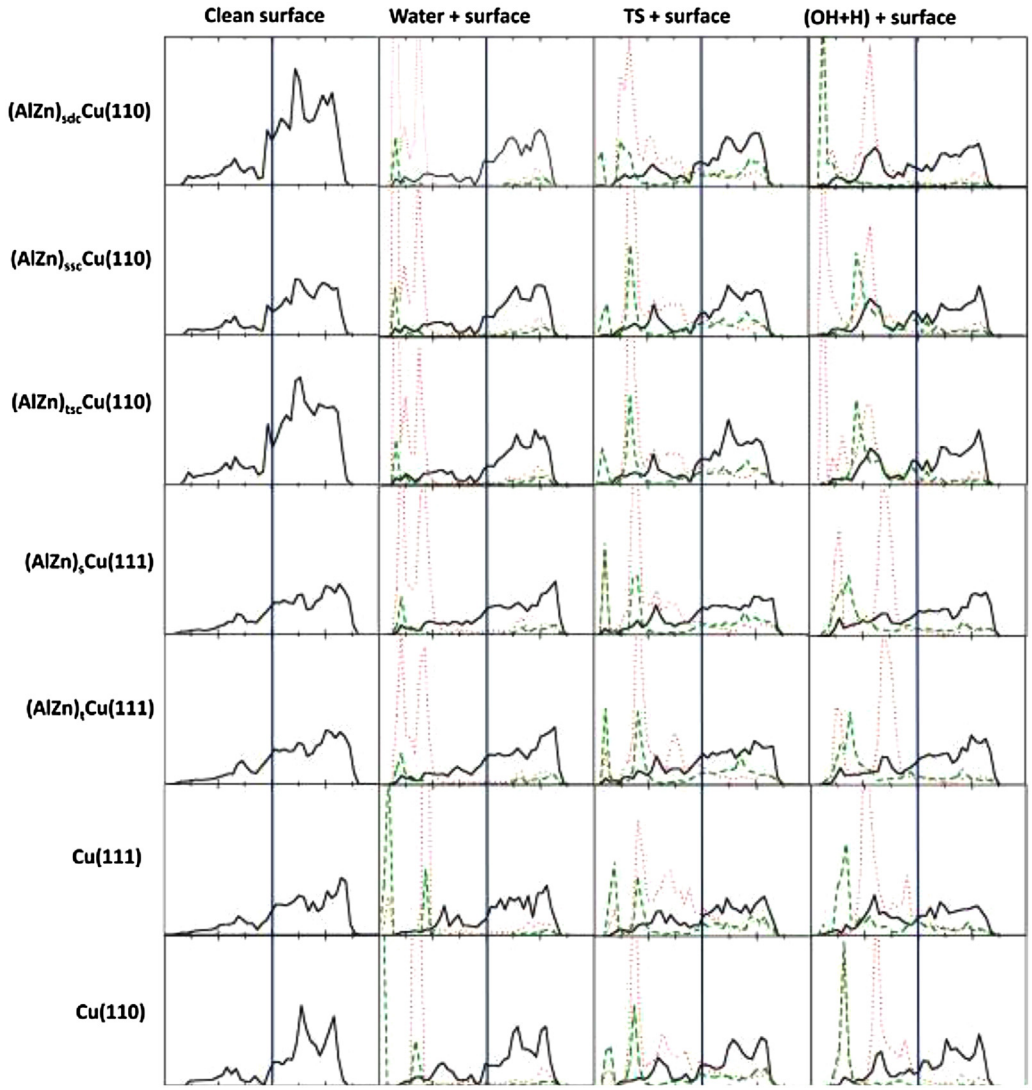

Fig. 3. Projected density of states (pDOS, arbitrary units) for the water dissociation on trimetallic surfaces. Solid black lines correspond to the d-band of the upmost metal surface atoms; dotted red lines correspond to the p-band of oxygen atoms and dashed green lines correspond to the s-band of the hydrogen atom suffering O—H bond cleavage. In all panels, the vertical blue line denotes the Fermi level. (For interpretation of the references to colour in this figure legend, the reader is referred to the web version of this article.)

case of trimetallic catalyst models. By comparison of computed and estimated data it was conclude that the BEP provides accurate estimates for the (111) flat surfaces while significant disagreement was found in the case of the (110) combed models.

Acknowledgments

This work was developed within the scope of the projects CICECO-Aveiro Institute of Materials, POCI-01-0145-FEDER-007679 (FCT UID/CTM/50011/2013), LAQV@REQUIMTE, POCI/01/0145/FEDER/007265, (FCT UID/QUI/50006/2013 and NORTE-01-0145-FEDER-000011), financed by national funds through the FCT/MEC and when appropriate co-financed by FEDER under the PT2020 Partnership Agreement. J.L.C.F. and J.R.B.G. acknowledge FCT for the grant SFRH/BPD/105650/2015, cofinanced by the Programa Operacional Potencial Humano (POPH)/Fundo Social Europeu (FSE) and Quadro de Referência Estratégico Nacional 2009–2013 do Governo da República Portuguesa, and for the Programme Investigador FCT, respectively. M.N.D.S.C. also acknowledges FCT/MEC for Grant SFRH/BSAB/127789/2016.

Appendix A. Supplementary data

Supplementary data associated with this article can be found, in the online version, at http://dx.doi.org/10.1016/j.apcatb.2017.06.050.

References

[1] X. Hu, L. Zhang, G. Lu, Int. J. Hydrogen Energy 41 (2016) 13960–13969.
[2] J.S. Yoo, H.T. Kim, H.-I. Joh, H. Kim, S.H. Moon, Int. J. Hydrogen Energy 36 (2011) 1930–1938.
[3] C. Brooks, S. Cypes, R.K. Grasselli, A. Hagemeyer, Z. Hogan, A. Lesik, G. Streukens, A.F. Volpe Jr., H.W. Turner, W.H. Weinberg, K. Yaccato, Topics Catal. 38 (2006) 195–209.
[4] S. Zafeiratos, F. Paloukis, G. Papakonstantinou, D. Teschner, M. Hävecker, E. Vass, P. Schnörch, A. Knop-Gericke, R. Schlögl, B. Moreno, E. Chinarro, J.R. Jurado, S.G. Neophytides, Catal. Today 157 (2010) 250–256.
[5] Materials Genome Initiative for Global Competitiveness. Executive Office of the President of United State of America; National Science and Technology Council, 2011 (November 2011. http://www.whitehouse.gov/sites/default/files/microsites/ostp/materials_genome_initiative-final.pdf.).
[6] J.L.C. Fajín, M.N.D.S. Cordeiro, F. Illas, J.R.B. Gomes, J. Catal. 276 (2010) 92–100.
[7] R.A. van Santen, M. Neurock, S.G. Shetty, Chem. Rev. 110 (2010) 2005–2048.
[8] J.L.C. Fajín, M.N.D.S. Cordeiro, J.R.B. Gomes, Chem. Comm. 47 (2011) 8403–8405.

[9] J.L.C. Fajín, M.N.D.S. Cordeiro, J.R.B. Gomes, J. Phys. Chem. C 116 (2012) 10120–10128.
[10] J.L.C. Fajín, M.N.D.S. Cordeiro, J.R.B. Gomes, App. Catal. A-Gen. 458 (2013) 90–102.
[11] J.L.C. Fajín, A. Bruix, M.N.D.S. Cordeiro, J.R.B. Gomes, F. Illas, J. Chem. Phys. 137 (2012), 034701-(1–10).
[12] R.B. Rankin, J. Greeley, ACS Catal. 2 (2012) 2664–2672.
[13] J.K. Nørskov, T. Bligaard, J. Rossmeisl, C.H. Christensen, Nat. Chem. 1 (2009) 37–46.
[14] J.K. Nørskov, T. Bligaard, B. Hvolbæk, F. Abild-Pedersen, I. Chorkendorff, C.H. Christensen, Chem. Soc. Rev. 37 (2008) 2163–2171.
[15] S. Wang, B. Temel, J. Shen, G. Jones, L. Grabow, F. Studt, T. Bligaard, F. Abild-Pedersen, C.H. Christensen, J.K. Nørskov, Catal. Lett. 141 (2011) 370–373.
[16] A. Vojvodic, F. Calle-Vallejo, W. Guo, S. Wang, A. Toftelund, F. Studt, J.I. Martínez, J. Shen, I.C. Man, J. Rossmeisl, T. Bligaard, J.K. Nørskov, F. Abild-Pedersen, J. Chem. Phys. 134 (2016), 244509(1–8).
[17] S. Wang, V. Petzold, V. Tripkovic, J. Kleis, J.G. Howalt, E. Skúlason, E.M. Fernández, B. Hvolbæk, G. Jones, A. Toftelund, H. Falsig, M. Björketun, F. Studt, F. Abild-Pedersen, J. Rossmeisl, J.K. Nørskov, T. Bligaard, Phys. Chem. Chem. Phys. 13 (2011) 20760–20765.
[18] J.L.C. Fajín, M.N.D.S. Cordeiro, F. Illas, J.R.B. Gomes, J. Catal. 268 (2009) 131–141.
[19] J.L.C. Fajín, M.N.D.S. Cordeiro, J.R.B. Gomes, J. Chem. Phys. 138 (2013), 074701-(1–9).
[20] J.L.C. Fajín, M.N.D.S. Cordeiro, F. Illas, J.R.B. Gomes, J. Catal. 313 (2014) 24–33.
[21] J.L.C. Fajín, F. Viñes, M.N.D.S. Cordeiro, F. Illas, J.R.B. Gomes, J. Chem. Theor. Comput. 12 (2016) 2121–2126.
[22] A. Gokhale, J.A. Dumesic, M. Mavrikakis, J. Am. Chem. Soc. 130 (2008) 1402–1414.
[23] H. Prats, P. Gamallo, F. Illas, R. Sayós, J. Catal. 342 (2016) 75–83.
[24] C.T. Campbell, Topics Catal. 1 (1994) 353–366.
[25] C.T. Campbell, ACS Catal. 7 (2017) 2770–2779.
[26] N. Schumacher, A. Boisen, S. Dahl, A.A. Gokhale, S. Kandoi, L.C. Grabow, J.A. Dumesic, M. Mavrikakis, I. Chorkendorff, J. Catal. 229 (2005) 265.
[27] L.V. Mattos, G. Jacobs, B.H. Davis, F.B. Noronha, Chem. Rev. 112 (2012) 4094–4123.
[28] A.Y. Rozovskii, G.I. Lin, Top. Catal. 22 (2003) 137–150.
[29] M.A. Larrubia-Vargas, G. Busca, U. Costantino, F. Marmottini, T. Montanari, P. Patrono, F. Pinzari, G. Ramis, J. Mol. Catal. A: Chem. 266 (2007) 188–197.
[30] S.H.D. Lee, D.V. Applegate, S. Ahmed, S.G. Calderone, T.L. Harvey, Int. J. Hydrogen Energy 30 (2005) 829–842.
[31] S. Boumaza, A. Auroux, S. Bennici, A. Boudjemaa, M. Trari, A. Bouguelia, R. Bouarab, Reac. Kinet. Mech. Cat. 100 (2010) 145–151.
[32] G. Kresse, J. Hafner, Phys. Rev. B 47 (1993) 558–561.
[33] G. Kresse, J. Furthmüller, Comput. Mater. Sci. 6 (1996) 15–50.
[34] G. Kresse, J. Furthmüller, Phys. Rev. B 54 (1996) 11169–11186.
[35] J.P. Perdew, J.A. Chevary, S.H. Vosko, K.A. Jackson, M.R. Pederson, D.J. Singh, C. Fiolhais, Phys. Rev. B 46 (1992) 6671–6687.
[36] P.E. Blöchl, Phys. Rev. B 50 (1994) 17953–17979.
[37] G. Kresse, D. Joubert, Phys. Rev. B 59 (1999) 1758–1775.
[38] H.J. Monkhorst, J.D. Pack, Phys. Rev. B 13 (1976) 5188–5192.
[39] J.F.C. Fajín, F. Illas, J.R.B. Gomes, J. Chem. Phys. 130 (2009) 224702.
[40] J.P. Perdew, K. Burke, M. Ernzerhof, Phys. Rev. Lett. 77 (1996) 3865–3868.
[41] H. Prats, P. Gamallo, R. Sayós, F. Illas, Phys. Chem. Chem. Phys. 18 (2016) 2792–2801.
[42] G. Henkelman, H. Jónsson, J. Chem. Phys. 111 (1999) 7010–7022.
[43] J.L. Ayastuy, M.A. Gutiérrez-Ortiz, J.A. González-Marcos, A. Aranzabal, J.R. González-Velasco, Ind. Eng. Chem. Res. 44 (2005) 41–50.
[44] K.J. Laidler, Chemical Kinetics, third, Harper Collins, New York, 1987, pp. 193.
[45] A.A. Phatak, W.N. Delgass, F.H. Ribeiro, W.F. Schneider, J. Phys. Chem. C 113 (2009) 7269–7276.